AIAA JOURNAL
Vol. 36, No. 9, September 1998

Pressure-Based Compressible Calculation Method Utilizing Total Variation Diminishing Schemes

R. I. Issa* and M. H. Javareshkian†
Imperial College of Science, Technology, and Medicine, London SW7 2BX, England, United Kingdom

A pressure-based implicit procedure to solve the Euler and Navier–Stokes equations on a nonorthogonal mesh with collocated finite volume formulation is described. The boundedness criteria for this procedure are determined from total variation diminishing (TVD) schemes, which are based on characteristic variables and are applied to the fluxes of the convected quantities, including mass flow rate. The procedure incorporates the k–ε eddy-viscosity turbulence model. The algorithm is first tested for inviscid flows at different Mach numbers ranging from subsonic to supersonic on a bump in a channel geometry, where the results are compared with other existing numerical solutions. The method is then validated against experiment and another numerical solution for the case of turbulent transonic flow through a gas turbine rotor blade cascade for which wind-tunnel experimental data exist. The comparisons show that the quality of the resolution of the TVD scheme, as implemented in the pressure-based procedure, is similar to that obtained when applied in density-based methods.

Nomenclature

$A, \tilde{D}, D$	= finite difference coefficients
a	= eigenvalues of the Jacobian matrix
$\tilde{a}$	= cell face area
C_μ, C_1, C_2	= empirical coefficients
F	= mass flux
G	= generation of turbulent kinetic energy
g	= flux limiter
I	= flux
k	= kinetic energy of turbulence
$\boldsymbol{q}$	= scalar flux vector
R	= right eigenvector matrix
T	= stress tensor
u, v	= mean (time-average) velocity components in x and y directions, respectively
α	= characteristic variable
Γ	= diffusivity coefficient
Γ_ϕ^t	= turbulent diffusivity coefficients
$\delta\upsilon$	= cell volume
ε	= volumetric rate of dissipation
ϵ	= small positive number
μ	= dynamic viscosity
μ_t	= turbulent viscosity
ρ	= density
σ_k	= turbulent Prandtl numbers for turbulent kinetic energy
σ_ε	= turbulent Prandtl numbers for dissipation rate
$\mathbf{\Phi}$	= vector containing the components of the antidiffusive flux terms
ϕ	= scalar quantity

Introduction

THE capturing of sharp gradients associated with shock waves and contact discontinuities has been the subject of much research and development. The work has resulted in the devising of various high-resolution bounded schemes, notably the total variation diminishing (TVD) technique.[1,2] Most of these schemes have been implemented in density-based numerical algorithms, which are specific to highly compressible flows. This imposes a restriction on the applicability of the methodology and precludes its use in multipurpose computational fluid dynamics procedures that can be applied to incompressible as well as compressible flows. Alternatively, pressure-based methods offer the capability of handling both of these classes of flow in a unified manner. Recently, several authors have implemented the TVD technique in pressure-based algorithms. Lien and Leschziner[3] introduced a MUSCL (Van Leer[4])-type of TVD scheme into their pressure-based procedure; the flux limiter in their work relies on the gradients of the solved-for dependent variables. A density-retardation technique, tantamount to upwinding on the pressure gradient, is introduced to account for the hyperbolic nature of the conservation equations. There is also the work of Shyy and Thakur,[5] who developed what they call the controlled variation scheme (CVS), which is based on the formalism of the TVD concept, introduced in the context of incompressible flow. Those authors expressed the view that existing TVD schemes do not generalize to pressure-based methods for two reasons.[5] The first is related to contemporary sequential-iteration methods of the solution, which treat the pressure gradients as source terms in the momentum equations; this is unlike simultaneous algorithms, which treat gradients as part of the flux vectors. The second reason is the lack of definition of local characteristics on which the flux limiters of the TVD schemes are based. Their CVS scheme was generalized to compressible flows containing shocks as well as incompressible flows by Thakur et al.[6]

In the cited works, the gradients of either the conserved or primitive variables are used in formulating the flux-limiting function. This is different from constructing the flux limiter on characteristic variables that are considered to be appropriate for compressible flow problems. Indeed, Mulder and Van Leer[7] and Lin and Chieng,[8] who carried out extensive numerical experiments, found that, at least for one-dimensional flow, the best accuracy was obtained by using the Riemann variables. This may be because only one of these variables will undergo a small change through a wave or a contact front, whereas large changes take place in conserved or primitive variables.

Issa and Javareshkian[9] were among the first to implement a high-resolution TVD scheme with characteristic-variables-based flux limiters into a pressure-based finite volume method that solves the Euler and Navier–Stokes equations. The scheme was applied to transient one-dimensional problems and to inviscid subsonic and transonic flows. The contribution of the present paper is to extend this scheme and apply it to new cases for which the results are compared against available experimental data and other numerical solutions; these include supersonic inviscid flow and transonic, turbulent flow through a blade passage.

Contemporary with the work of Issa and Javareshkian[9] are the works of Kobayashi and Pereira[10] and Batten et al.,[11] where characteristic-based flux computations were introduced into pressure-correction solution procedures. Kobayashi and Pereira[10] use the

Received May 30, 1997; revision received April 20, 1998; accepted for publication April 23, 1998.

*Reader, Department of Mechanical Engineering.
†Research Student, Department of Mechanical Engineering.

essentially nonoscillating scheme for the flux calculation, which they incorporated into a steady-state solution method. Batten et al. utilized the TVD approach and adopted a time marching technique. In contrast, the method presented herein has been incorporated in both transient mode[9] and a steady-state mode.

Governing Equations and Descretization

The basic equations, which describe the conservation of mass, momentum, and scalar quantities, can be expressed in Cartesian tensor form as

$$\frac{\partial \rho}{\partial t} + \frac{\partial (\rho u_j)}{\partial x_j} = 0 \tag{1}$$

$$\frac{\partial (\rho u_i)}{\partial t} + \frac{\partial (\rho u_j u_i - T_{ij})}{\partial x_j} = S_i^u \tag{2}$$

$$\frac{\partial (\rho \phi)}{\partial t} + \frac{\partial (\rho u_j \phi - \boldsymbol{q}_j)}{\partial x_j} = S^\phi \tag{3}$$

The stress tensor and scalar flux vector are usually expressed in terms of basic dependent variables. The stress tensor for a Newtonian fluid is

$$T_{ij} = -p\delta_{ij} - \frac{2}{3}\mu \frac{\partial u_k}{\partial x_k}\delta_{ij} + \mu\left(\frac{\partial u_i}{\partial x_j} + \frac{\partial u_j}{\partial x_i}\right) \tag{4}$$

The scalar flux vector is usually given by a Fourier-type law:

$$\boldsymbol{q}_j = \Gamma_\phi \left(\frac{\partial \phi}{\partial x_j}\right) \tag{5}$$

In the preceding equations, the velocities and scalar variables are taken to be density-weighted, i.e., Favre, ensemble averages.

Turbulence is accounted for by adopting the k–ε turbulence model. The governing equations for these quantities are

$$\frac{\partial}{\partial t}(\rho k) + \frac{\partial}{\partial x_j}\left(\rho u_j k - \Gamma_k \frac{\partial k}{\partial x_j}\right) = G - \rho\varepsilon + D_{\text{comp}} + \Theta_{\text{diff}} \tag{6}$$

$$\frac{\partial}{\partial t}(\rho \varepsilon) + \frac{\partial}{\partial x_j}\left(\rho u_j \varepsilon - \Gamma_k \frac{\partial \varepsilon}{\partial x_j}\right) = C_1 \frac{\varepsilon}{k} G - C_2 \rho \frac{\varepsilon^2}{k} \tag{7}$$

The turbulent viscosity and diffusivity coefficients are defined by

$$\mu_t = C_\mu \rho (k^2/\varepsilon) \tag{8}$$

$$\Gamma_\phi^t = \left(\mu_t \big/ \sigma_\phi^t\right) \tag{9}$$

and the generation term G in Eqs. (6) and (7) is defined by

$$G = \mu_t \left[\left(\frac{\partial u_i}{\partial x_j} + \frac{\partial u_j}{\partial x_i}\right)\frac{\partial u_i}{\partial x_j} - \frac{2}{3}\delta_{ij}\left(\frac{\partial u_m}{\partial x_m} + \rho k\right)\frac{\partial u_i}{\partial x_j}\right] \tag{10}$$

The terms D_{comp} and Θ_{diff} are additional contributions to the standard k–ε model often introduced to account for the effects of compressibility.[12,13] In this work, the models proposed by Yang et al.[12] are adopted, namely,

$$D_{\text{comp}} = -\frac{9}{55}\rho k \frac{\partial u_i}{\partial x_i} - \frac{1}{\rho}\cdot\frac{\mu_t}{\rho}\cdot\frac{\partial \rho}{\partial x_i}\cdot\frac{\partial p}{\partial x_i} \tag{11}$$

$$\Theta_{\text{diff}} = 0 \tag{12}$$

the latter being appropriate for high-Reynolds-number flows, as is the case here.

The values of the turbulence model coefficients used in the present work are given in Table 1.

Table 1 Values of empirical coefficients in the standard k–ε turbulence model

C_1	C_2	C_μ	σ_k	σ_ε
1.44	1.92	0.09	1.0	1.3

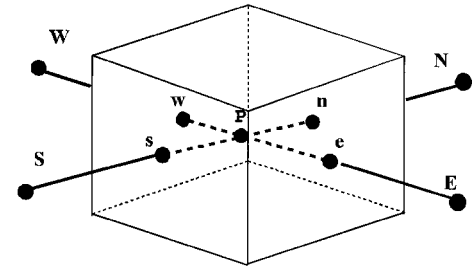

Fig. 1 Finite volume and storage arrangement.

The preceding conservation equations are discretized through integration over control volumes such as that shown in Fig. 1. The development of the discrete expressions to be presented is effected with reference to only one face of the control volume, namely, e, for the sake of brevity.

For any variable ϕ (which may now also stand for the velocity components), the result of the integration yields

$$\frac{\delta \upsilon}{\delta t}\left[(\rho\phi)_p^{n+1} - (\rho\phi)_p^n\right] + I_e - I_w + I_n - I_s = S_\phi \delta \upsilon \tag{13}$$

where I is the combined cell-face convection I_C and diffusion I_D fluxes. The diffusion flux is approximated by central differences and can be written as an example for cell-face e of the control volume in Fig. 1 as

$$I_{D,e} = \tilde{D}_e(\phi_P - \phi_E) - S_e^\phi \tag{14}$$

where S_e^ϕ stands for cross derivatives arising from mesh nonorthogonality. The expression for the convective fluxes (mass, momentum, and energy) are determined by the TVD scheme used for interpolation from the nodes at the neighboring points, for example, nodes E and P. The expression can be written, in general, as

$$I_{C,e}^l = \tfrac{1}{2}\left[I_{C,p}^l + I_{C,E}^l + R_e \Phi_e^l\right] \tag{15}$$

where $R_e\Phi_e$ is a dissipation term based on the characteristic field decomposition of the flux difference. The superscript l denotes the various fluxes concerned, i.e., mass momentum component and energy. Thus, for example, for the u component of the momentum, the convective flux is written as

$$I_{C,e} = \tfrac{1}{2}\left[F_E u_E + F_P u_P + \tfrac{1}{2}[p_E \cdot \delta y_E + p_P \cdot \delta y_P] + \tfrac{1}{2}\left[R_e \phi_e^{ux} \cdot \delta y_e - R_e \phi_e^{uy} \cdot \delta x_e\right]\right] \tag{16}$$

where F is the mass flux.

According to Yee et al.,[2] a spatially second-order upwind formula for the components of $\boldsymbol{\Phi}_e$ is given by

$$\phi_e^1 = \tfrac{1}{2}\psi\left(a_e^l\right)\left(g_P^l + g_E^l\right) - \psi\left(a_e^l + \gamma_e^l\right)\alpha_e^l \tag{17}$$

The flux limiter g may be defined in any way chosen. For the present work, the MINMOD limiter due to Harten[1] is used; thus,

$$g_P^l = \min \mathrm{mod}\left(a_e^l - a_w^l\right) \tag{18}$$

where

$$\min \mathrm{mod}(x, y) = \mathrm{sign}(x) \cdot \max\{0, \min[|x|, y\,\mathrm{sign}(x)]\}$$

The spatial increments of the characteristic variables are obtained from

$$\alpha_e^l = R_e^{-1}\left(\phi_E^l - \phi_P^l\right) \tag{19}$$

For γ one can take[2]

$$\gamma_e^l = \frac{1}{2}\psi\left(\alpha_e^l\right)\begin{cases} \dfrac{g_E^l - g_P^l}{\alpha_e^l}, & \alpha_e^l \neq 0 \\ 0, & \alpha_e^l = 0 \end{cases} \tag{20}$$

The function ψ is required to prevent nonphysical solutions, such as expansion shocks, and introduces a small amount of dissipation. Following the suggestion of Harten and Hyman,[14] it is taken as

$$\begin{aligned} \psi(z) &= (z^2/4\epsilon) + \epsilon \qquad \text{for} \qquad |z| < 2\epsilon \\ &= |z| \qquad\qquad\quad \text{for} \qquad |z| \geq 2\epsilon \end{aligned} \tag{21}$$

where ϵ is an arbitrary small number. With the preceding assumption, the discretized equations take the form

$$A_P \phi_P = \sum_{m=E,W,N,S} A_m \phi_m + S'_\Phi \tag{22}$$

where the A are coefficients whose expressions are given as

$$\begin{aligned} A_E &= D_e - (F_E/2), \qquad A_N = D_n - (F_N/2) \\ A_W &= Dw - (F_W/2), \qquad A_S = D_s - (F_S/2) \end{aligned} \tag{23}$$

with

$$A_P = A_E + A_W + A_N + A_S + (\rho \delta \upsilon / \delta t)$$

The term S'_Φ in Eq. (22) contains quantities arising from nonorthogonality, numerical dissipation terms, external sources, and $(\rho \delta \upsilon / \delta t)\phi_p$ of the old time-step/iteration level. For the momentum equations it is easy to separate out the pressure-gradient source from the convected momentum fluxes given by expressions such as Eq. (16).

Solution Algorithm

The set of Eq. (22) is solved for the primitive variables (velocity components and energy) together with continuity utilizing pressure-based implicit sequential solution methods. The techniques used are either the PISO scheme for time-dependent problems[9] or the SIMPLE scheme for the steady-state problems presented herein. In both of these techniques, the methodology has to be adapted to handle the way in which the fluxes are computed in Eqs. (15–20).

The adapted SIMPLE scheme consists of a predictor and corrector sequence of steps at every iteration. The predictor step solves the implicit momentum equation using the old pressure field. Thus, for example, for the u component of velocity, the momentum predictor stage can be written as

$$u^* = H(u^*) - D \nabla p^0 + S'_u \tag{24}$$

where H contains all terms relating to the surrounding nodes and superscripts $*$ and 0 denote intermediate and previous iteration values, respectively. Note that the pressure-gradient term is now written out explicitly; it is extruded from the total momentum flux by simple subtraction and addition. The corrector-step equation can be written as

$$u^{**} = H(u^*) - D \nabla p^* + S'_u \tag{25}$$

Hence, from Eqs. (24) and (25),

$$u^{**} - u^* = -D \nabla (p^{**} - p^*), \qquad \text{or} \qquad \delta u = -D \nabla \delta p \tag{26}$$

Now the continuity equation demands that

$$\nabla(\rho^* u^{**}) = 0 \tag{27}$$

for steady-state flows. For compressible flows it is essential to account for the effect of change of density on the mass flux as the presure changes. This is accounted for by linearizing the mass fluxes as follows (as in Ref. 15):

$$\rho^* u^{**} \approx \rho^0 u^* + \rho^0 \delta u + u^* \delta \rho \tag{28}$$

or

$$\rho^* u^{**} \approx \rho^0 u^* - \rho^0 D \nabla \delta p + u^* \left(\frac{\mathrm{d}\rho}{\mathrm{d}p} \right) \delta p \tag{29}$$

where Eq. (26) is invoked to eliminate δu and $\delta \rho$ is related to δp by the appropriate equation of state. Substitution of Eq. (29) into Eq. (27) yields a pressure-correction equation of the form

$$A_p \cdot \delta p_p^* = A_E \cdot \delta p_E^* + A_W \cdot \delta p_W^* + A_N \cdot \delta p_N^* + A_S \cdot \delta p_S^* + S_p \tag{30}$$

where S_p is the finite difference analog of $\nabla(\rho^0 u^*)$, which vanishes when the solution is converged.

The A coefficients in Eq. (30) take the form (the expression for A_E is given as an example)

$$A_E = (\rho^0 \tilde{a} D)_e - \lambda_e (\tilde{a} u^*)_e \cdot \left(\frac{\mathrm{d}\rho}{\mathrm{d}p} \right)_e \tag{31}$$

where λ is a factor whose significance is explained subsequently.

Because the mass flux at a cell face is computed directly [via Eq. (15)] from nodal values of density and velocity, the cell-face values of ρ_e^0 and u_e^* in Eq. (31) are not readily available. To compute those values, assumptions concerning the variations of ρ need to be made. For example, if upwinding is chosen, then λ would take the value of 1 when u is positive; otherwise it would be zero. Alternatively, if a central difference formula is used, then $\lambda = \frac{1}{2}$. It is important to recognize, however, that such assumptions have no influence whatsoever on the final solution because they affect only the pressure-correction coefficients, and as δp goes to zero at convergence, the solution is, therefore, independent of how those coefficients are formulated; however, they do influence the convergence behavior. What is important is how $\nabla(\rho^0 u^*)$ in Eq. (30) is computed (as this does determine the solution), and this is based on the TVD principle outlined earlier.

The structure of the coefficients in Eq. (30) simulates the hyperbolic nature of the equation system. Indeed, a closer inspection of expression (31) would reveal an upstream bias of the coefficients (A decreases as u increases), and this bias is proportional to the square of the Mach number. Also note that the coefficients reduce identically to their incompressible form in the limit of zero Mach number.

The overall solution procedure follows the same steps as in the standard SIMPLE algorithm, with the exception of solving the hyperbolic-like pressure-correction equation (30). To ensure convergence of the iterative process, underrelaxation factors between 0.1 and 0.2 for pressure correction and between 0.2 and 0.5 for the other variables are employed.

Boundary Conditions

At the inlet of the domain, all flow variables are specified if the flow is supersonic. For subsonic inlet flow, only three of the four variables need to be prescribed: the total temperature, the angle of attack, and the total pressure. The pressure is obtained by zeroth-order extrapolation from interior points. At outlet, all of the flow variables are obtained by linear extrapolation for supersonic velocities; the pressure is fixed when the outlet is subsonic. Slip boundary conditions are used on the lower and upper walls of the bump in the inviscid flow test cases. In the case of viscous flow, the no-slip condition is applied at the solid walls. To account for the steep variations in turbulent boundary layers near solid walls, wall functions, which define the velocity profile in the vicinity of no-slip boundaries, are employed.[16]

Also, numerical boundary conditions have to be formulated for the flux limiters. According to Yee[17] there are three choices of boundary values for the g_i^l function in Eq. (17). In the present work, the g_i^l function on a boundary face has been approximated by $\alpha_{i+3/2}^l$, which has the smallest dissipative value among the three possible choices.

Results

Both two-dimensional inviscid and viscous flows are computed, and the results are compared either with existing numerical solutions obtained by others or with experimental data where available. The first validation is the flow over a bump in a channel geometry in which subsonic, transonic, and supersonic flows were computed and compared with other existing numerical predictions, including TVD schemes in density-based methods. It is then validated for a two-dimensional viscous flow through a gas turbine rotor blade

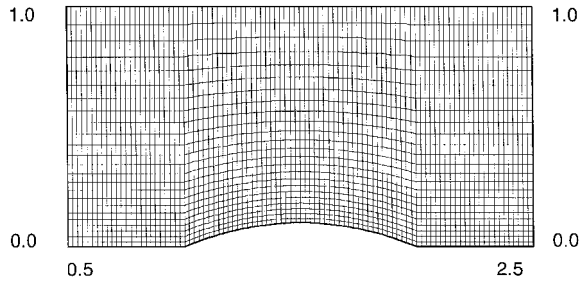

a) Bump geometry

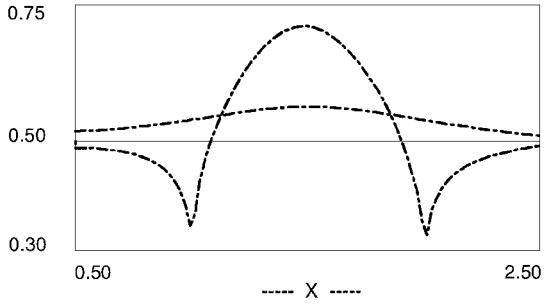

b) Mach number on walls

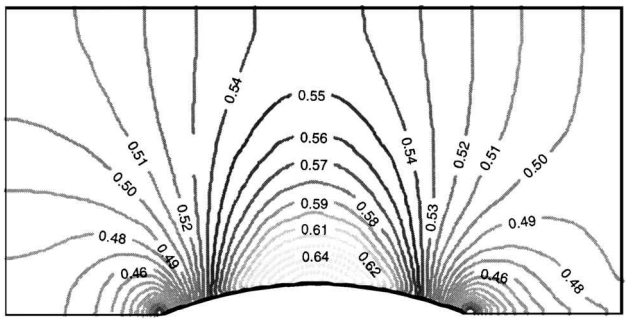

c) Mach contours

Fig. 2 Subsonic flow over 10% thick bump, inlet $M = 0.5$.

cascade for which wind-tunnel experimental data exist, and the results are compared with the measurements and another numerical solution.

In Fig. 2a the geometry of a 10% thick bump on a channel wall is shown together with the mesh used (98 × 25) to compute steady two-dimensional inviscid flow. Three cases were considered for this geometry, one with inlet Mach number of 0.5 resulting in a subsonic flow throughout, another with inlet Mach number of 0.675 leading to transonic flow over the bump, and the third case with inlet Mach number of 1.6.

Figures 2b and 2c present, respectively, the Mach number distribution on the walls and isomach lines for the case of $M_{-\infty} = 0.5$. As shown in Fig. 2, the numerical solution is quite symmetric about the midchord, which is a good indication of solution accuracy for this subsonic application.

Figure 3 presents the results of transonic flow in a similar geometry (Fig. 2a). The grid dependence test for this flow is indicated in Fig. 3a. As can be seen, the results of these meshes do not change much, indicating that an acceptable solution can be obtained even on the coarse mesh. The Mach number and pressure distributions on the lower and upper walls for two different TVD schemes are shown in Figs. 3b and 3c. Widerman and Iwamoto[18] used a density-based method with a simultaneous explicit solver. The agreement between the two solutions is close, thus verifying the validity of the present TVD generalization. An indication of the shock resolution is offered by Fig. 3d, where constant pressure contours are displayed.

Figures 4 and 5 present solutions for two supersonic flows ($M_{-\infty} = 1.6$ and 1.4) past 10% and 4% thick circular arc bumps in a channel, respectively. The results of two TVD schemes on a grid of 98 × 25 nodes, that of Widermann and Iwamoto[18] and of the present TVD scheme, are shown in Figs. 4a and 4b for the $M_{-\infty} = 1.6$ case.

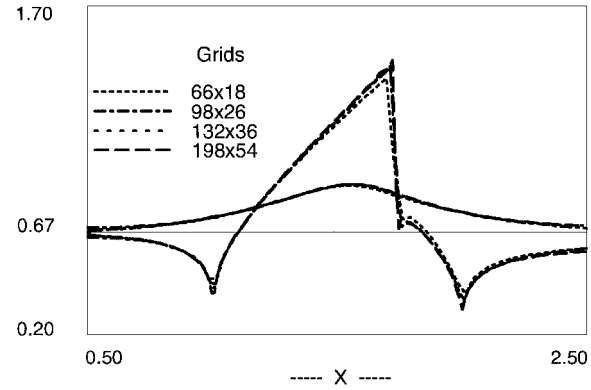

a) Mach number on walls: grid dependence test

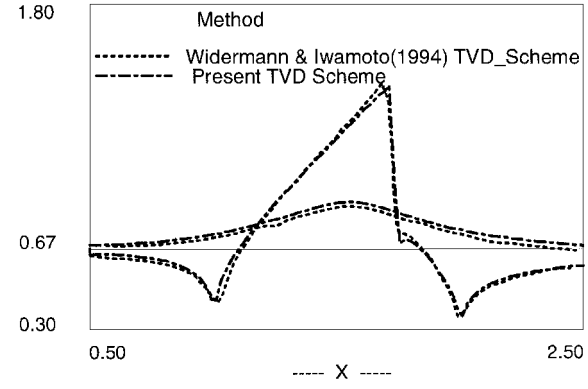

b) Mach number on walls: comparison with density-based method

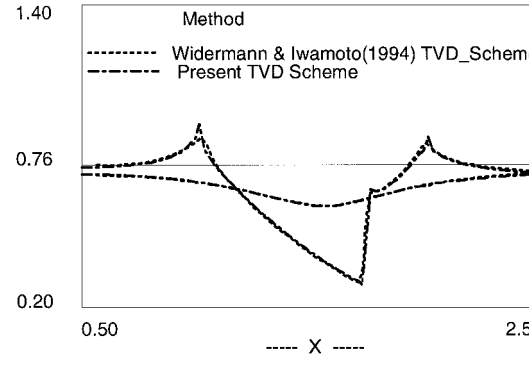

c) Pressure ratio on walls

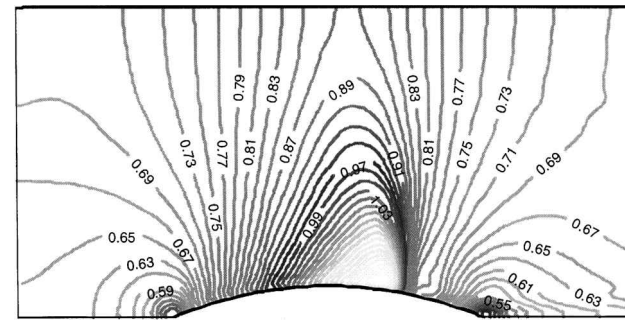

d) Mach contours

Fig. 3 Transonic flow over 10% thick bump, inlet $M = 0.675$.

The Mach number and pressure distributions on the lower and upper walls are chosen to compare the resolution of shock waves for these schemes. The comparisons indicate that both the reflection of the leading-edge shock on the upper wall and the trailing-edge shock are captured with the same sharpness, but the present TVD scheme has a sharper leading-edge shock with the consequence of predicting a lower Mach number over the bump. Figure 4c shows the predicted Mach number distribution. Figure 5a shows the predicted Mach

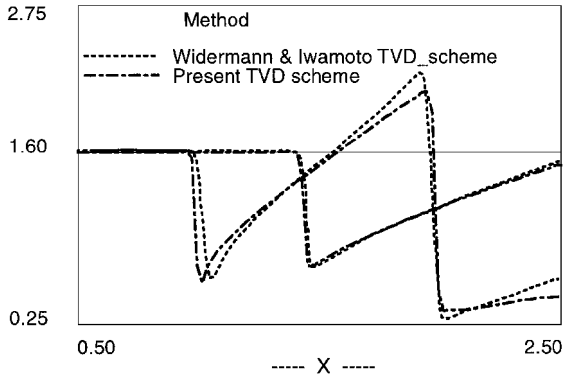

a) Mach number on walls

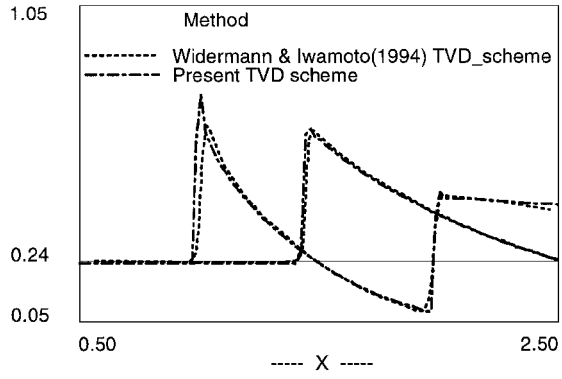

b) Pressure ratio on walls

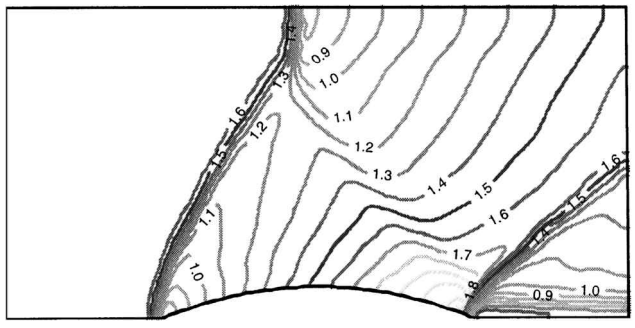

c) Mach contours (present TVD)

Fig. 4 Supersonic flow over 10% bump.

number distribution for the case of $M_{-\infty} = 1.4$. The results of Lien and Leschziner,[3] who approximated the advective fluxes using the quadratic scheme QUICK or a second-order TVD scheme operating on the primitive variables, on a grid of 90×30 nodes are compared with the present scheme in Fig. 5b, where the Mach number distributions on the lower and upper walls are shown. The Lien and Leschziner[3] scheme apparently predicts sharper shocks; however, closer inspection of Fig. 5 shows that this is achieved at the cost of the presence of over- and undershoots in the solution. This is very likely to be the result of not using the Riemann variables in the TVD scheme. The present second-order TVD scheme on the other hand predicts bounded solutions in the vicinity of the shock at the cost of a slight decrease in sharpness of resolution. In any event, shock sharpness is a function of the limiter used (MINMOD in this case) and is independent of the implementation that is the subject of the present paper. Other limiters (such as SUPERBEE[19]) could be used in the present method,[9] and they might have produced sharper shock resolution. Indeed, the results of Kobayashi and Pereira[10] with the MINMOD limiter for a similar case show correspondence with the quality of the present results; those authors[10] also showed that marked improvement in resolution could be obtained by use of different flux limiters. Batten et al.[11] also show that good shock capturing resolution can be achieved by a different choice of TVD limiter.

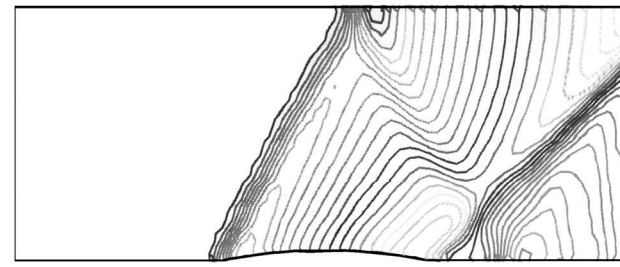

a) Mach contours (present TVD scheme)

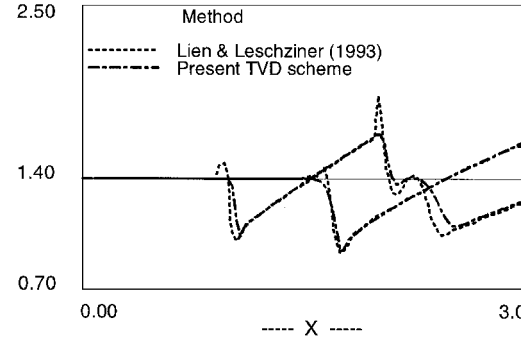

b) Mach number on walls

Fig. 5 Supersonic flow over 4% thick bump.

Figure 6 presents the solution for the turbulent flow past the von Kármán Institute (VKI) gas turbine rotor blades. The flow is turned through 96 deg by the blades and exits to a downstream static pressure corresponding to an isentropic Mach number of 1.2.

The domain of the solution is confined to one blade passage, and cyclic boundary conditions are employed to simulate the repeating flow pattern from one passage to the next. At the inlet, the total pressure and temperature were specified, whereas the static pressure corresponding to the isentropic exit Mach number was prescribed. The turbulence quantities were specified at inlet to correspond to 1% turbulence intensity and a dissipation length scale of 10% of the blade pitch.

Grid independence studies were performed on H grids of 130×31, 228×31, 228×58, and 299×58 nodes, respectively. Care was taken such that the y^+ values of the nodes next to the walls were well above 20 to maintain validity of the wall functions used. The results of this study[20] show that reasonable mesh independence was attained on the 228×58 grid, for which the results are presented here.

Figure 6a shows the basic H-grid layout and the iso-Mach line distribution. Figure 6b presents a comparison between the present TVD scheme and that of Arnone et al.,[21] who used a C grid of 449×33 nodes and a density-based method with an explicit solver. They also used the Baldwin–Lomax[22] turbulence model that was developed for boundary-layer calculations; the present calculations use the k–ε model. From Fig. 6 it is observed that the pressure-side distribution of the isentropic Mach number and the shock definition are nearly the same for the two schemes, and both methods predict the shock position ahead of the actual location due to the shock/boundary-layer interaction, which leads to a sudden growth of the boundary layer around that region. As it is seen from these results, there is quite a good agreement between the present predictions and the measurement of Sieverding[23] at VKI, with the exception of the overexpansions at the rounded trailing edge. This unrealistic overexpansion may be due to failure to capture the true geometry of the trailing edge. (Although H-type grids are easy to generate, they provide poor leading- and trailing-edge definition.) Indeed, Arnone et al.[21] could improve their results by adding a fictitious solid wedge to the trailing edge of the blade to simulate a recirculation zone. The turbulence model and wall functions cannot deal adequately with the interaction taking place between the shock wave and the boundary layer. In view of all of these shortcomings, it is remarkable, therefore, that reasonable agreement with the data is obtained on such a relatively coarse mesh.

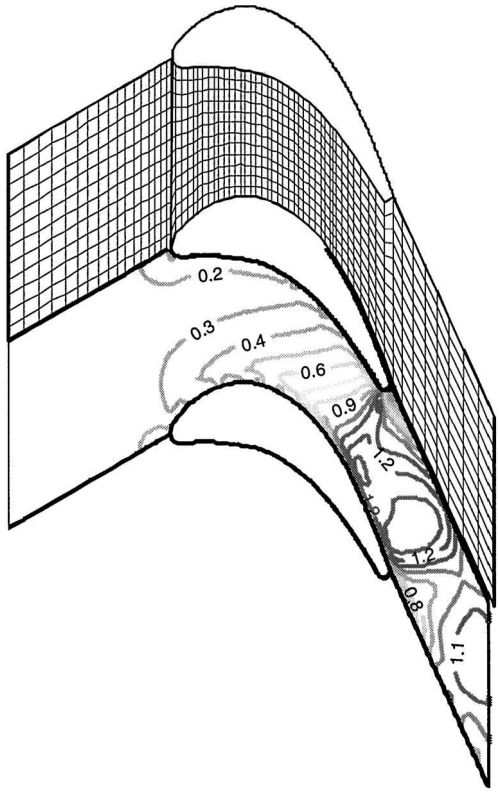

a) Iso-Mach lines and grid

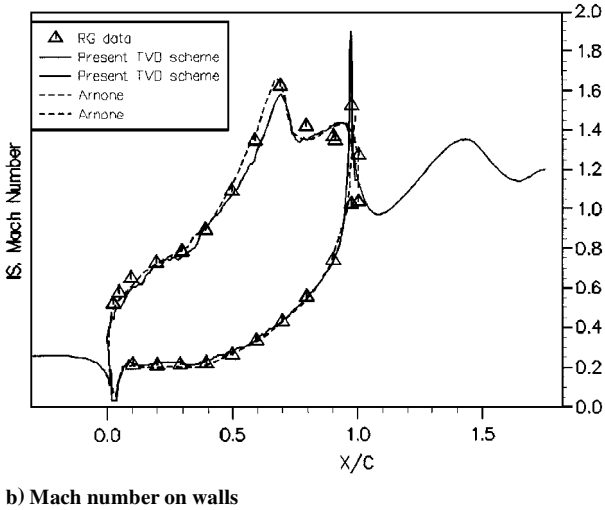

b) Mach number on walls

Fig. 6 Transonic flow in the VKI turbine rotor blade passage.

Conclusion

A pressure-based implicit procedure has been described that incorporates bounded high resolution of discontinuities and is, therefore, well suited to all flow ranging from subsonic to supersonic. The boundedness criteria for this procedure are determined from TVD schemes, which are applied to the fluxes of the convected quantities, including mass flow. The flux limiter is based on the characteristic variables. The main findings can be summarized as follows:

1) The agreement between the results of the present implementation of TVD schemes and other implementations of the same limiter, using density-based methods, is excellent, as it should be.

2) The TVD scheme based on characteristic variables produces a smooth solution around discontinuities, unlike those using the primitive variables, which can give some over- or undershoots.

3) The grid dependence test of the inviscid test case indicates that an acceptable solution can be obtained even on fairly coarse meshes, verifying the practicability of the method for engineering applications.

4) Application of the method to turbulent flow in a blade passage validates the implementation in frictional flow.

References

[1]Harten, A., "High Resolution Scheme for Hyperbolic Conservation Laws," *Journal of Computational Physics*, Vol. 49, No. 3, 1983, pp. 357–393.

[2]Yee, H. C., Warming, R. F., and Harten, A., "Implicit Total Variation Diminishing (TVD) Schemes for Steady State Calculations," *Journal of Computational Physics*, Vol. 57, No. 2, 1985, pp. 327–360.

[3]Lien, F. S., and Leschziner, M. A., "A Pressure-Velocity Solution Strategy for Compressible Flow and Its Application to Shock Boundary-Layer Interaction Using Second-Moment Turbulence Closure," *Journal of Fluids Engineering*, Vol. 115, No. 4, 1993, pp. 717–725.

[4]Van Leer, B., "Towards the Ultimate Conservation Difference Scheme. II. Monotonicity and Conservation Combined in Second Order Scheme," *Journal of Computational Physics*, Vol. 14, No. 4, 1974, pp. 361–370.

[5]Shyy, W., and Thakur, S., "Controlled Variation Scheme in a Sequential Solver for Recirculating Flows," *Heat Transfer*, Vol. 25, No. 3, Pt. B, 1994, pp. 273–286.

[6]Thukur, S., Wright, J., Shyy, W., Liu, J., Ouyang, H., and Vu, T., "Development of Pressure-Based Composite Multigrid Methods for Complex Fluid Flows," *Progress in Aerospace Sciences*, Vol. 32, No. 4, 1996, pp. 313–375.

[7]Mulder, W. A., and Van Leer, B., "Experiments with Implicit Upwind Methods for the Euler Equations," *Journal of Computational Physics*, Vol. 59, 1985, pp. 232–246.

[8]Lin, H., and Chieng, C. C., "Characteristic-Based Flux Limiters of an Essentially Third-Order Flux-Splitting Method for Hyperbolic Conservation Laws," *International Journal for Numerical Methods in Fluids*, Vol. 13, No. 3, 1991, pp. 287–307.

[9]Issa, R. I., and Javareshkian, M. H., "Application of TVD Schemes in Pressure-Based Finite-Volume Methods," *Proceedings of the Fluids Engineering Division Summer Meeting*, Vol. 3, American Society of Mechanical Engineers, New York, 1996, pp. 159–164.

[10]Kobayashi, M. H., and Pereira, J. C. F., "Characteristic-Based Pressure Correction at all Speeds," *AIAA Journal*, Vol. 34, No. 2, 1996, pp. 272–280.

[11]Batten, P., Lien, F. S., and Leschziner, M. A., "A Positivity-Preserving Pressure-Correction Method," Proceedings of 15th International Conf. on Numerical Methods in Fluid Dynamics, Monterey, CA, 1996.

[12]Yang, Z. Y., Chin, S. B., and Swithenbank, J., "On the Modeling of the k-Equation for Compressible Flow," 7th International Symposium on Numerical Methods in Laminar and Turbulent Flow, Stanford, CA, July 1991.

[13]Narayan, J. R., and Sekar, B., "Computation of Turbulent High Speed Mixing Layers Using a Two-Equation Turbulence Model," CFD Symposium on Aeropropulsion, NASA CP-3078, Jan. 1991.

[14]Harten, A., and Hyman, J. M., "Self Adjusting Grid Methods of One-Dimensional Hyperbolic Conservation Laws," *Journal of Computational Physics*, Vol. 50, 1983, pp. 235–269.

[15]Karki, K. C., and Patankar, S. V., "Pressure-Based Calculation Procedure for Viscous Flows at All Speeds in Arbitrary Configurations," *AIAA Journal*, Vol. 27, No. 9, 1989, pp. 1167–1174.

[16]Launder, B. E., and Spalding, D. B., "The Numerical Computation of Turbulent Flows," *Computer Methods in Applied Mechanics and Engineering*, Vol. 3, 1974, p. 269.

[17]Yee, H. C., "Numerical Experiments with a Systematic High-Resolution Shock-Capturing Scheme," NASA TM-88325, June 1986.

[18]Widermann, A., and Iwamoto, J., "A Multigrid TVD-Type Scheme for Computing Inviscid and Viscous Flows," *Computer and Fluids*, Vol. 23, No. 5, 1994, pp. 711–735.

[19]Roe, P. L., "Some Contributions to the Modeling of Discontinuous Flows," *Lectures in Applied Mathematics*, Vol. 22, Society of Industrial and Applied Mathematics, 1985, pp. 163–193.

[20]Javareshkian, M. H., "High Resolution Difference Schemes for Steady and Transient Compressible Flow," Ph.D. Thesis, Mechanical Engineering, Imperial College, Univ. of London, London, Nov. 1996.

[21]Arnone, A., Liou, M. S., and Povinelli, L. A., "Transonic Cascade Flow Calculation Using Non-Periodic C-Type Grid," CFD Symposium on Aeropropulsion, NASA CP-3078, Jan. 1991, pp. 143–162.

[22]Baldwin, B. S., and Lomax, H., "Thin Layer Approximation and Algebraic Model for Separated Turbulent Flows," AIAA Paper 78-0257, 1978.

[23]Sieverding, C., "Transonic Flows in Turbomachinery," Von Kármán Inst. for Fluid Dynamics, LS-59, Rhode St. Genese, Belgium, 1973.

W. Oberkampf
Associate Editor